small methods

www.small-methods.com

A Versatile Scanning Photocurrent Mapping System to Characterize Optoelectronic Devices based on 2D Materials

Christoph Reuter, Riccardo Frisenda, Der-Yuh Lin, Tsung-Shine Ko, David Perez de Lara, and Andres Castellanos-Gomez**

The investigation of optoelectronic devices based on 2D materials and their heterostructures is a very active area of investigation with both fundamental and applied aspects involved. Here, a description of a home-built scanning photocurrent microscope is presented, which is designed and developed to perform electronic transport and optical measurements of 2D-materials-based devices. The complete system is rather inexpensive (<10 000 €) and it can be easily replicated in any laboratory. To illustrate the setup, current–voltage characteristics are measured, in the dark and under global illumination, of an ultrathin p–n junction formed by the stacking of an n-doped few-layer MoS_2 flake onto a p-type MoS_2 flake. Scanning photocurrent maps are then acquired, and by mapping the short-circuit current generated in the device under local illumination, it is found that at zero bias, the photocurrent is generated mostly in the region of overlap between the n-type and p-type flakes.

Motivated by their remarkable electronic properties, recently there has been a surge of experimental efforts to apply graphene and other 2D materials, such as transition-metal dichalcogenides (TMDCs), black phosphorous (BP), and others in electronic devices such as field-effect transistors, logic circuits, oscillators, or flash memories.[1–6] The fabrication of heterostructures based on the stacking of different 2D materials has also shown promising results in the fabrication of rectifiers and more complex devices.[7,8] Apart from presenting outstanding electronic properties, some of these materials (TMDCs, BP) can interact strongly with light and are considered prospective candidates for novel optoelectronics devices.[9,10] In fact, in the last few years, 2D-based detectors with ultrahigh responsivity,[11] atomically thin solar cells,[12] and ultrafast photodetectors[13] among others, have been demonstrated.

In most previous studies, the characteristics of 2D-based optoelectronic devices were studied upon wide-field illumination (light spot larger than the device lateral dimensions) which is fast to implement and gives valuable information like the responsivity or the time constant of the device.[14,15] Nevertheless, given the rich plethora of mechanisms involved in the photocurrent generation process in 2D systems, some physical effects cannot be studied in this kind of measurements. Therefore, scanning photocurrent (SPC) measurements, where a small-diameter light spot is scanned over the device area to spatially resolve the photocurrent generation, have been carried out to better understand the working principles behind 2D-based optoelectronic devices.[12,16–21] Among the different SPC studies found in the literature, we mention the investigation of the Schottky barriers generated at the interface between TMDCs and metallic electrodes,[22–25] photothermoelectric effects in MoS_2,[26] and the band-offsets at monolayer–multilayer MoS_2 junctions.[27] These studies have clearly demonstrated how SPC mapping is a very powerful tool in the investigation of optoelectronic devices based on 2D materials. We found, however, that a comprehensive description of the tools and the setup employed to carry out these experiments is missing in the literature (including in Ph.D. dissertations) which is probably hampering the widespread implementation of this useful technique. Moreover, the standard way used in the literature to carry out SPC measurements is to employ an optical chopper to modulate the incident light and a lock-in amplifier to record the modulated photocurrent.[19,28] This measurement scheme has the advantage of allowing the measurement of small electrical signals, for example, in samples with a low responsivity and high dark current, given the large achievable signal to noise ratio, while two main disadvantages are the high price of the lock-in amplifier and the large optical table needed to accommodate the necessary components.

In this context, we present a thorough description of a home-built scanning photocurrent microscope that we have designed and developed. The complete system is rather inexpensive (<10 000 €) and it can be easily replicated (see **Table 1** for a full list with all the required components and their part numbers).

C. Reuter
Department of Electrical Engineering and Information Technology
Technische Universität Ilmenau
Gustav-Kirchhoff-Str. 1, Ilmenau 98693, Germany

C. Reuter, Dr. R. Frisenda, Dr. D. Perez de Lara,
Dr. A. Castellanos-Gomez[+]
Instituto Madrileño de Estudios Avanzados en Nanociencia
(IMDEA-nanociencia)
Campus de Cantoblanco
E-28049, C/Faraday 9, Madrid, Spain
E-mail: riccardo.frisenda@imdea.org; andres.castellanos@csic.es

Prof. D.-Y. Lin, Prof. T.-S. Ko
Department of Electronic Engineering
National Changhua University of Education
No. 2, Shi-Da Rd, Changhua City 500, Taiwan, Republic of China

[+]Present address: Instituto de Ciencia de Materiales de Madrid
(ICMM-CSIC), C/Sor Juana Inés de la Cruz 3, E-28049 Madrid, Spain

DOI: 10.1002/smtd.201700119

 © 2017 WILEY-VCH Verlag GmbH & Co. KGaA, Weinheim

Table 1. Components of the scanning photocurrent setup with indicated the part number, the distributor, and the commercial price.

Part number	Description	Distributor	Price [€]
	Zoom-lens tube + focus stage + PCB camera + LED illuminator	Hongkong Lapsun Kits (ebay)	475.00
716-2040	Breadboard table, 400 mm × 200 mm	EKSMA optics	130.00
CCM1-BS 013/M	50/50 beam splitter cube	Thorlabs	241.20
SM1A9	External C-mount to internal SM1 adapter	Thorlabs	16.88
SM1NR1	Focusing ring	Thorlabs	175.50
CXY1	*XY* manual adjustment of light spot	Thorlabs	152.15
M530F2	Fiber-coupled 530 nm LED	Thorlabs	333.00
LEDD1B	T-Cube LED driver	Thorlabs	263.70
KPS101	LED driver power supply	Thorlabs	23.14
M65L01	10 µm-diameter core fiber	Thorlabs	99.90
M28L01	400 µm-diameter core fiber	Thorlabs	75.69
960-0070-03LS	Motorized translation stage	EKSMA optics	2 × 498.00
980-0942	2-axis translational stage controller	EKSMA optics	940.00
	Keithley 2450 sourcemeter	Keithley	5000.00
56650	2× Conversion lens	Edmund optics	191.10
RP01/M	Rotation stage	Thorlabs	82.53
PB1	Mounting post base	Thorlabs	21.33
P300/M	Ø1.5″ Mounting post, L = 300 mm	Thorlabs	71.10
RS300/M	Ø25.0 mm Mounting post, L = 300 mm	Thorlabs	50.75

We illustrate the performance of the present setup by acquiring scanning photocurrent maps in an ultrathin p–n junction formed by the stacking of an n-doped few-layer MoS_2 flake onto a p-type MoS_2 flake, demonstrating state-of-the-art performance. We thus believe that we provide a simple yet powerful tool that can be implemented in many groups working on the optoelectronic properties of graphene and other 2D materials.

The setup is based on a zoom-lens inspection system with coaxial illumination, depicted in **Figure 1**. A 50:50 beam splitter has been attached to the C-mount camera port of the lens tube. A USB CMOS camera is connected to one of the ports of the beam splitter while the other port is used as an input of the illumination that is going to be focused onto a small-diameter spot on the sample, which is brought into the zoom lens through a multimode fiber. The spot illumination port is equipped with a focusing ring that allows one to modify the position of the optical fiber until the fiber core end is exactly placed at the image plane of the lens system. Under this condition, an image of the circular fiber core end (reduced accordingly to the magnification of the lens) is projected onto the surface of the sample. Therefore, one can easily adjust the diameter of the spot illumination by either selecting a multimode fiber with a desired core diameter or by modifying the magnification of the zoom-lens system. The relationship between the fiber core diameter and the projected illumination spot diameter is given in Figure S1 and S2 of the Supporting Information. The spot illumination port is also supplemented with an *xy* manual stage that allows one to move the position of the spot in the sample plane, being a useful addition for the initial alignment of the spot in the camera's field of view. The source of the spot illumination can be any fiber-coupled light source. In our implementation, we have chosen high-power fiber-coupled light-emitting diodes (LEDs) because they are inexpensive and safe to use and their light intensity can be manually controlled or modulated up to 5 kHz with an external signal generator.

The sample is mounted on a rotational sample holder fixed on a motorized *xy* stage. The two motorized axes have a travel range of 25 mm with a resolution of 1.25 µm in full steps and 0.156 µm in 1/8 steps with a maximum speed of 6 mm s^{-1}. The *xy* stage can be controlled through a USB driver unit, connected to the computer. Whilst scanning the sample, illuminated by a high-power LED spot, the device electrical properties are measured with a Keithley 2450 source meter unit as a function of the spot position. The data acquisition and motion control are managed through a home-made routine written in Matlab. A crucial part of the scanning photocurrent measurements is to correlate the photogenerated current with the device geometry. To do so, other SPC mapping systems replace the camera during the scanning by a photodiode. The signal measured by the photodiode, which is proportional to the local reflectivity of the sample, is recorded at each step of the scan, simultaneously to the current, to provide a reflectivity map used to correlate the photocurrent map and the device geometry. In our system, we employ directly the signal from the USB camera to construct the reflectivity map. To do so, at each step of the scan, we record a snapshot with the camera and we extract the intensity of the spot in the Matlab program. An example of the reflection map construction is given in Figure S4 of the Supporting Information.

Figure 1a shows pictures of the different components of the SPC system and Figure 1b displays a schematic drawing. In Figure S3 and S5 of the Supporting Information further detailed pictures of the experimental setup are provided. In order to facilitate the implementation of this setup by others, Table 1 lists the different components indicating their part number and vendor. To illustrate the performances of this setup we characterize a p–n junction, fabricated by stacking n-doped MoS_2 flake (MoS_2 with 0.5% of Fe substitutional atoms corresponding to a density of approximately 3×10^{19} atoms cm^{-3}) on top of a p-doped MoS_2 flake (0.5% Nb doping) by means of an all-dry transfer method, which is schematically depicted in **Figure 2**a. More details about the fabrication and the characteristics of these p–n junction devices can be found in Figure S6 and S7 of the Supporting Information and in ref. [29]. From a microscopy image of the device, we extract the flakes overlap area, $A_{p-n} = (135 \pm 5)$ µm^2.

We first characterize the device under global illumination selecting an optical fiber with a large core (400 µm) that yields a spot on the surface of the sample with a diameter of 33 µm (area $A_{Spot} = 3421$ µm^2 >> A_{p-n}) that is larger than the device dimensions. The light source is a fiber-coupled high-power green LED (λ = 530 nm). Figure 2b displays current–voltage (I–V) characteristics of the device in dark conditions and under increasing illumination power densities (see Figure S8 of the Supporting

© 2017 WILEY-VCH Verlag GmbH & Co. KGaA, Weinheim

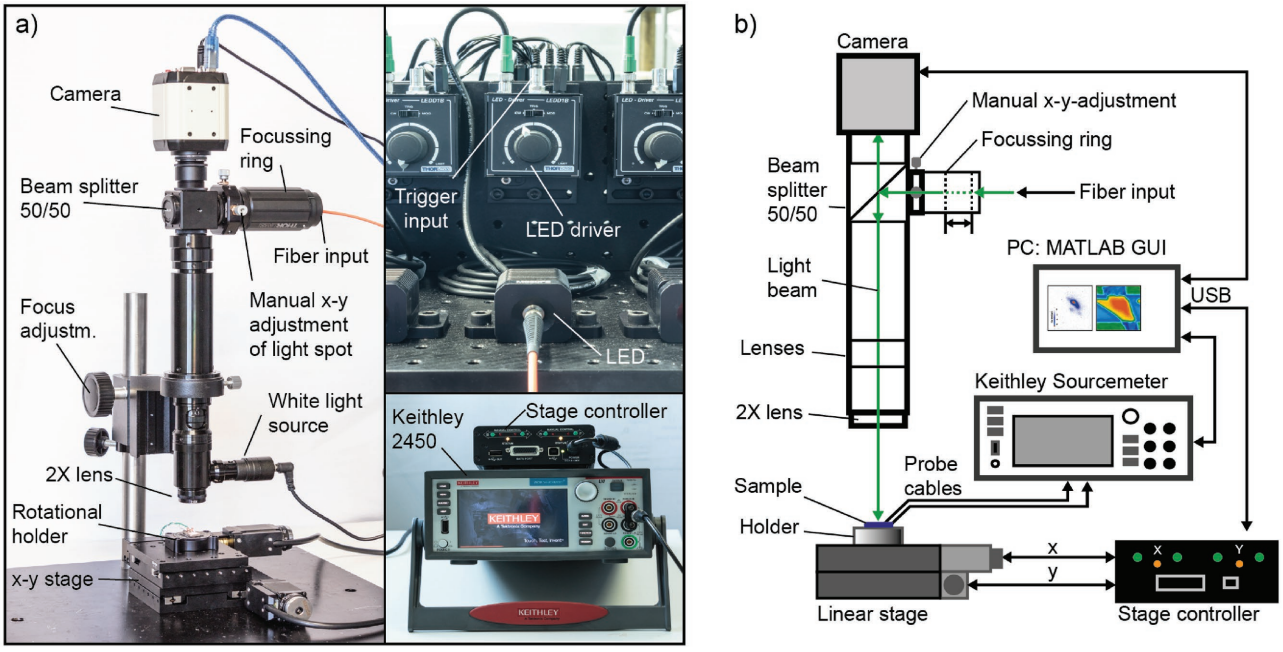

Figure 1. a) Pictures of the components of the scanning photocurrent setup with the main components indicated. b) Schematics of the setup circuitry and of the optical path.

Information for a logarithmic representation of the *I*–*V*). From an inspection of the *I*–*V* relationship, one can see that the device behaves as a diode with a maximum rectification in dark of 250 at 1 V. Upon illumination the forward current increases due to photoconductive effect reaching a saturation current of 0.7 μA at the largest incident power density of 14 mW cm^{-2}. The time dependence of the photocurrent under different bias conditions is shown in Figure S9 of the Supporting Information. At zero applied bias voltage, the built-in potential at the p–n junction can effectively separate the photogenerated electron–hole pair giving rise to a photocurrent at zero bias voltage (commonly known as the short-circuit current, I_{SC}). Similarly, a voltage builds up across the junction at zero current upon illumination (open-circuit voltage, V_{OC}). These two parameters can directly be extracted from the *I*–*V* under illumination, as shown in the inset of Figure 2b. Figure 2c shows I_{SC} and V_{OC} plotted as a function of the incident optical power. It can be seen that I_{SC} follows a linear dependency on the power while V_{OC} has a logarithmic dependence, as confirmed by fits, consistent with the classical model of a p–n junction. The MoS_2 p–n junction can be used as a solar cell and Figure S10, in the Supporting Information, shows the electrical power that can

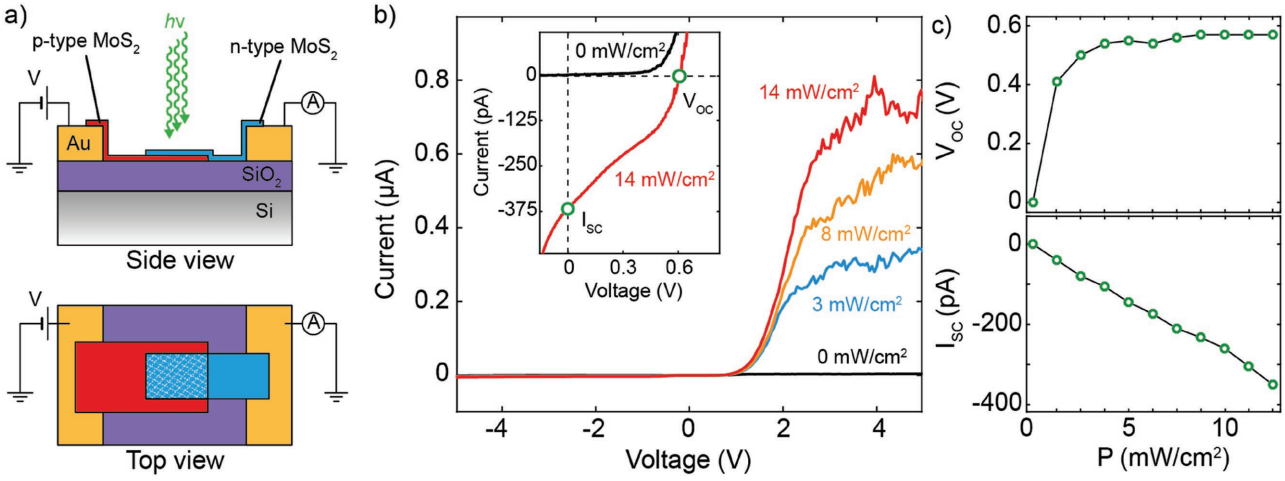

Figure 2. a) Schematics of the p–n junction based on an n-type doped MoS_2 flake stacked on top of a p-type MoS_2 flake. b) Current–voltage characteristics of the device in dark conditions (black line) and under external illumination with different power densities ($\lambda = 530$ nm). Inset: current–voltage curves at low-bias with indicated the solar cell parameters. c) Open-circuit voltage (top) and short-circuit current (bottom) as a function of the illumination power density extracted from current–voltage characteristics.

© 2017 WILEY-VCH Verlag GmbH & Co. KGaA, Weinheim

be extracted from the device as a function of the illumination power density. At a power density of 14 mW cm^{-2}, the open-circuit voltage is V_{OC} = 0.57 V and the maximum generated power is P_{MP} = 75 pW at a voltage V_{MP} = 0.42 V. From these values we find the figures of merit of the MoS_2 p–n junction: fill factor F.F. = 0.52 and efficiency η = 0.5%.

We now turn our attention to SPC mapping measurements carried out in the same device. To probe locally the device, we replace the 400 µm core multimode optical fiber with a 10 µm core one to produce a spot on the sample surface of (2.3 ± 0.3) µm of diameter, defined as the full width at half maximum of the Gaussian shaped intensity spot profile. This value for the spot size is approximately two times larger than the theoretical diffraction-limited spot size of 1.1 µm given the numerical aperture of our setup N.A. = 0.25. This suggests that additional broadening of the spot is present eventually due to imperfections in the tube lens (see the Supporting Information). To increase the resolution of the setup, one could replace the present lens tube (N.A. = 0.25) with one with a larger numerical aperture or to switch to a confocal microscope arrangement. A different approach is to abandon the far-field regime and work in near-field, for example, in the near-field optical scanning microscopy (SNOM) technique.[16,17,30–32] Nevertheless, we notice that both these approaches would result in higher setup costs and a more complex experimental arrangement in respect to focusing and alignment than the proposed solution.

Figure 3a shows an optical image of the region of the sample investigated by SPC mapping where one can distinguish the drain and source gold electrodes and the two stacked MoS_2 flakes that are partially overlapping. By mapping the photocurrent while the drain–source voltage is kept at zero, one maps the short-circuit current I_{SC}. The misalignment between the bands of the two differently doped MoS_2 flakes generates locally an electric potential that can separate the photoexcited electron–hole pairs and give rise to a net current. This process is expected to take place only in the region where the p-type and n-type flakes overlap.[12,21] During the SPC measurement, we block any external light that could hit the sample, apart from the focused laser used to scan.

Figure 3b shows the recorded zero-bias current (I_{SC}) map that has been acquired simultaneously to the reflectivity map (Figure 3c) using a step-size of 0.5 µm in both directions. The slow-scan axis is parallel to the *y*-axis while the fast-scan axis is parallel to the *x*-axis in the image. By inspecting the color map of Figure 3b one can see that a (negative) photocurrent, indicated by the blue/red color, is generated only in the region of overlap between the two MoS_2 flakes (see Figure S11 of the Supporting Information for a saturated color map that facilitate this observation). The rest of the sample does not display photogeneration of current, evidenced by the white color. Notice that the current recorded when the laser spot is located far away from the MoS_2 flakes or from the electrodes corresponds exactly to the dark current of the sample. By subtracting the dark current from the total current recorded in each position one can find the photocurrent generated by the sample.

Interestingly, the photocurrent generation is not homogeneous across the whole overlapping region, but, instead, a hot-spot where I_{SC} reaches 6.4 pA is visible. We attribute this spatial inhomogeneous current photogeneration to nonuniform interlayer interaction between the two stacked MoS_2 flakes as their interface may contain polymer contaminants or physisorbed adsorbates eventually trapped during the dry-transfer process. The active area of the device A_D, identifiable from the photocurrent generation in Figure 3b, appears to be smaller than the overlap area A_{p-n}. Thus, the efficiency calculated in precedence could be underestimated by a factor $A_{p-n}/A_D \approx 2$ which, if taken into account, gives an efficiency η = 1%. These measurements show the importance of spatially resolved photocurrent maps to deeply understand the performance and the limitations of 2D-based optoelectronic devices.

In summary, we have presented a scanning photocurrent setup that can be used to map the photoresponse of optoelectronic devices based on 2D materials and that can be operated in a global illumination mode and with local illumination (spot size down to 2 µm). We have described the system details and we have provided a full list of all the components part numbers to facilitate the implementation of this setup by others. We demonstrate the performance of this setup by mapping the zero-bias photocurrent generated in an n-type MoS_2/p-type MoS_2 p–n junction.

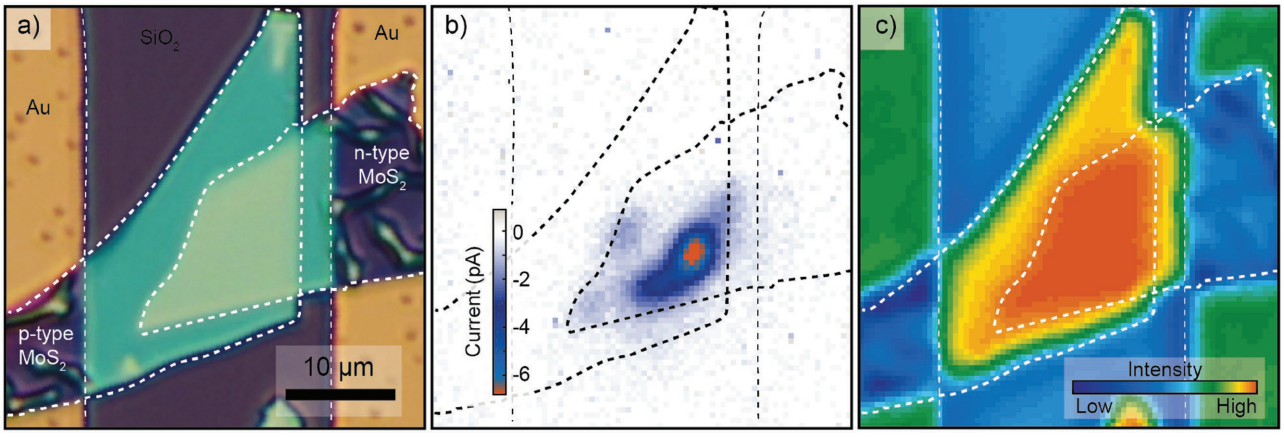

Figure 3. a) Optical image of the device. b) Photocurrent image of the MoS_2 p–n junction with zero bias voltage applied. c) Spatial map of the intensity of the reflected light from the device.

© 2017 WILEY-VCH Verlag GmbH & Co. KGaA, Weinheim

Supporting Information

Supporting Information is available from the Wiley Online Library or from the author.

Acknowledgements

A.-C.G. acknowledges financial support from the European Commission under the Graphene Flagship (contract no. CNECTICT-604391), the MINECO (Ramón y Cajal 2014 program RYC-2014-01406 and program MAT2014-58399-JIN), the Comunidad de Madrid (MAD2D-CM program (S2013/MIT-3007)). R.F. acknowledges funding from the Netherlands Organisation for Scientific Research (NWO) (Rubicon 680-50-1515). D.P.dL. was supported by the MINECO (program FIS2015-67367-C2-1-p). C.R. was supported by the German Academic Exchange Service (DAAD) through their RISE-program. D.-Y.L and T.-S.K. acknowledge financial support from the Ministry of Science and Technology of the Republic of China (MOST 105-2112-M-018-006 and MOS 105-2221-E-018-025).

Conflict of Interest

The authors declare no conflict of interest.

Keywords

2D materials, MoS_2, optoelectronics, p–n junctions, scanning photocurrent microscopy, solar cells, van der Waals heterostructures

Received: February 24, 2017
Revised: April 9, 2017
Published online: May 29, 2017

[1] Q. H. Wang, K. Kalantar-Zadeh, A. Kis, J. N. Coleman, M. S. Strano, *Nat. Nanotechnol.* **2012**, *7*, 699.
[2] G. Fiori, F. Bonaccorso, G. Iannaccone, T. Palacios, D. Neumaier, A. Seabaugh, S. K. Banerjee, L. Colombo, *Nat. Nanotechnol.* **2014**, *9*, 768.
[3] A. Castellanos-Gomez, *J. Phys. Chem. Lett.* **2015**, *6*, 4280.
[4] A. K. Geim, *Science* **2009**, *324*, 1530.
[5] S. Z. Butler, S. M. Hollen, L. Cao, J. A. Gupta, H. R. Gutierrez, T. F. Heinz, S. S. Hong, J. Huang, A. F. Ismach, *ACS Nano* **2013**, *7*, 2898.
[6] X. Ling, H. Wang, S. Huang, F. Xia, M. S. Dresselhaus, *Proc. Natl. Acad. Sci. USA* **2015**, *112*, 4523.
[7] A. K. Geim, I. V. Grigorieva, *Nature* **2013**, *499*, 419.
[8] K. Novoselov, A. C. Neto, *Phys. Scr.* **2012**, *2012*, 014006.
[9] F. Koppens, T. Mueller, P. Avouris, A. C. Ferrari, M. S. Vitiello, M. Polini, *Nat. Nanotechnol.* **2014**, *9*, 780.
[10] A. Castellanos-Gomez, *Nat. Photonics* **2016**, *10*, 202.
[11] B. Radisavljevic, A. Radenovic, J. Brivio, V. Giacometti, A. Kis, *Nat. Nanotechnol.* **2011**, *6*, 147.
[12] C.-H. Lee, G.-H. Lee, A. M. van der Zande, W. Chen, Y. Li, M. Han, X. Cui, G. Arefe, C. Nuckolls, T. F. Heinz, *Nat. Nanotechnol.* **2014**, *9*, 676.
[13] F. Xia, T. Mueller, Y.-M. Lin, A. Valdes-Garcia, P. Avouris, *Nat. Nanotechnol.* **2009**, *4*, 839.
[14] J. Ahn, P. J. Jeon, S. R. A. Raza, A. Pezeshki, S.-W. Min, D. K. Hwang, S. Im, *2D Mater.* **2016**, *3*, 045011.
[15] M. M. Furchi, D. K. Polyushkin, A. Pospischil, T. Mueller, *Nano Lett.* **2014**, *14*, 6165.
[16] A. Woessner, M. B. Lundeberg, Y. Gao, A. Principi, P. Alonso-González, M. Carrega, K. Watanabe, T. Taniguchi, G. Vignale, M. Polini, *Nat. Mater.* **2015**, *14*, 421.
[17] A. Woessner, P. Alonso-González, M. B. Lundeberg, Y. Gao, J. E. Barrios-Vargas, G. Navickaite, Q. Ma, D. Janner, K. Watanabe, A. W. Cummings, T. Taniguchi, V. Pruneri, S. Roche, P. Jarillo-Herrero, J. Hone, R. Hillenbrand, F. H. Koppens, *Nat. Commun.* **2016**, *7*, 10783.
[18] B. W. H. Baugher, H. O. H. Churchill, Y. Yang, P. Jarillo-Herrero, *Nat. Nanotechnol.* **2014**, *9*, 262.
[19] J. Park, Y. H. Ahn, C. Ruiz-Vargas, *Nano Lett.* **2009**, *9*, 1742.
[20] L. Britnell, R. M. Ribeiro, A. Eckmann, R. Jalil, B. D. Belle, A. Mishchenko, Y.-J. Kim, R. V. Gorbachev, T. Georgiou, S. V. Morozov, *Science* **2013**, *340*, 1311.
[21] F. Xia, T. Mueller, R. Goliazdeh-Mojarad, M. Freitag, Y.-M. Lin, J. Tsang, V. Perebeinos, P. Avouris, *Nano Lett.* **2009**, *9*, 1039.
[22] Y. Yi, C. Wu, H. Liu, J. Zeng, H. He, J. Wang, *Nanoscale* **2015**, *7*, 15711.
[23] N. Ubrig, S. Jo, H. Berger, A. F. Morpurgo, A. B. Kuzmenko, *Appl. Phys. Lett.* **2014**, *104*, 171112.
[24] C.-C. Wu, D. Jariwala, V. K. Sangwan, T. J. Marks, M. C. Hersam, L. J. Lauhon, *J. Phys. Chem. Lett.* **2013**, *4*, 2508.
[25] H. Yamaguchi, J. C. Blancon, R. Kappera, S. Lei, S. Najmaei, B. D. Mangum, G. Gupta, P. M. Ajayan, J. Lou, M. Chhowalla, J. J. Crochet, A. D. Mohite, *ACS Nano* **2015**, *9*, 840.
[26] M. Buscema, M. Barkelid, V. Zwiller, H. S. J. van der Zant, G. A. Steele, A. Castellanos-Gomez, *Nano Lett.* **2013**, *13*, 358.
[27] S. L. Howell, D. Jariwala, C.-C. Wu, K.-S. Chen, V. K. Sangwan, J. Kang, T. J. Marks, M. C. Hersam, L. J. Lauhon, *Nano Lett.* **2015**, *15*, 2278.
[28] R. Graham, D. Yu, *Mod. Phys. Lett. B* **2013**, *27*, 1330018.
[29] S. A. Svatek, E. Antolín, D.-Y. Lin, R. Frisenda, C. Reuter, A. J. Molina-Mendoza, M. Muñoz, N. Agrait, T.-S. Ko, D. Perez de Lara, A. Castellanos-Gomez, *J. Mater. Chem. C* **2016**, *5*, 854.
[30] F. Keilmann, R. Hillenbrand, *Philos. Trans. R. Soc., A* **2004**, *362*, 787.
[31] W. Bao, N. J. Borys, C. Ko, J. Suh, W. Fan, A. Thron, Y. Zhang, A. Buyanin, J. Zhang, S. Cabrini, P. D. Ashby, A. Weber-Bargioni, S. Tongay, S. Aloni, D. F. Ogletree, J. Wu, M. B. Salmeron, P. J. Schuck, *Nat. Commun.* **2015**, *6*, 7993.
[32] N. Rauhut, M. Engel, M. Steiner, R. Krupke, P. Avouris, A. Hartschuh, *ACS Nano* **2012**, *6*, 6416.

 © 2017 WILEY-VCH Verlag GmbH & Co. KGaA, Weinheim